Geochemistry, Geophysics, Geosystems®

RESEARCH ARTICLE
10.1029/2021GC010234

Precipitation and Lake Water Evaporation Recorded by Terrestrial and Aquatic *n*-Alkane δ^2H Isotopes in Lake Khar Nuur, Mongolia

Paul Strobel[1], Julian Struck[1], Enkhtuya Bazarradnaa[2], Michael Zech[3], Roland Zech[1], and Marcel Bliedtner[1]

[1]Institute of Geography, Friedrich Schiller University Jena, Jena, Germany, [2]Institute of Plant and Agricultural Sciences, Mongolian University of Life Sciences, Ulaanbaatar, Mongolia, [3]Heisenberg Chair of Physical Geography with Focus on Paleoenvironmental Research, Institute of Geography, Technische Universität Dresden, Dresden, Germany

Key Points:

- The hydrogen isotopic composition of terrestrial C_{31} *n*-alkanes reflects the local growing season precipitation at Lake Khar Nuur
- Aquatic C_{23} *n*-alkanes incorporate the isotopic signal of the lake's water, which is strongly modulated by evaporative enrichment
- The isotopic offset between C_{23} and C_{31} is a valuable proxy for evaporation in the lake and past hydrological changes in the catchment

Correspondence to:
P. Strobel,
paul.strobel@uni-jena.de

Citation:
Strobel, P., Struck, J., Bazarradnaa, E., Zech, M., Zech, R., & Bliedtner, M. (2022). Precipitation and lake water evaporation recorded by terrestrial and aquatic *n*-alkane δ^2H isotopes in Lake Khar Nuur, Mongolia. *Geochemistry, Geophysics, Geosystems*, *23*, e2021GC010234. https://doi.org/10.1029/2021GC010234

Received 28 OCT 2021
Accepted 26 JAN 2022

Author Contributions:
Conceptualization: Paul Strobel, Julian Struck, Marcel Bliedtner
Formal analysis: Paul Strobel, Marcel Bliedtner
Investigation: Paul Strobel, Marcel Bliedtner
Writing – original draft: Paul Strobel, Marcel Bliedtner
Writing – review & editing: Julian Struck, Enkhtuya Bazarradnaa, Michael Zech, Roland Zech

Abstract The compound-specific hydrogen isotopic composition (δ^2H) of *n*-alkanes is a valuable proxy to investigate hydrological conditions in lake sediments. While terrestrial *n*-alkanes reflect the isotopic signal of the local precipitation, aquatic *n*-alkanes incorporate the isotopic signal of the lake's water, which can be strongly modulated by evaporative enrichment. So far, the spatial distribution of the terrestrial and aquatic δ^2H signal within lakes have not systematically been investigated. Here, we present compound-specific δ^2H results of terrestrial (δ^2H_{C31}) and aquatic (δ^2H_{C23}) *n*-alkanes of surface sediment samples from Lake Khar Nuur, a semi-arid and high-altitude lake in the Mongolian Altai, and additionally investigate the δ^2H signal of topsoils from the catchment. Our results show that the majority of the *n*-alkane δ^2H values from the catchment topsoils correspond well with modeled local growing season precipitation (JJAS). However, few samples in the northern catchment show more positive δ^2H values possibly due to increased evapo(transpi)ration by southward exposition and shallower soils there. The only small variability of δ^2H_{C31} in the surface sediments is in the range of most topsoils δ^2H from the catchment, and thus, well reflects local growing season precipitation. δ^2H_{C23} in surface sediment samples from the central and deepest parts of the lake, that is, the lake's sediment accumulation zones, shows distinctly more positive δ^2H_{C23} values due to evaporative lake water enrichment. Consequently, $\Delta_{aq\text{-}terr}$, which is the isotopic offset between δ^2H_{C23} and δ^2H_{C31}, indicates distinct lake water enrichment in the lake's accumulation zones and is a valuable proxy to investigate past hydrological changes.

1. Introduction

The compound-specific hydrogen isotopic composition (δ^2H) of *n*-alkanes has been widely used for paleohydrological reconstructions in lacustrine sediments (e.g., Aichner et al., 2019; Thomas et al., 2016; Wirth & Sessions, 2016). Lacustrine sediments comprise terrestrial and aquatic *n*-alkanes, whose primary hydrogen source is the environmental water used for biosynthesis (Sachse et al., 2004; Xia et al., 2008). Terrestrial *n*-alkanes (e.g., C_{31}) mainly derive from the leaf waxes of higher terrestrial plants and primarily incorporate the local precipitation of the growing season as their source water for photosynthesis (Sachse et al., 2012; Strobel et al., 2021; Struck et al., 2020; Zech et al., 2015). The δ^2H signal of precipitation depends on atmospheric moisture pathways, temperature and the amount of precipitation (Bliedtner et al., 2020; Feakins & Sessions, 2010; Strobel et al., 2020). Additionally, fractionation processes can occur at the plant-soil interface, with evaporation of soil water and transpiration of leaf water being prominent factors (Feakins & Sessions, 2010; Kahmen et al., 2013; Zech et al., 2015). In contrast, aquatic *n*-alkanes (e.g., C_{23}) produced by algae and aquatic macrophytes incorporate the δ^2H signal of the lake's water (Ficken et al., 2000; Sachse et al., 2004; Strobel et al., 2021). While the lake water integrates the δ^2H signal of precipitation throughout the year, environmental factors such as temperature, salinity, nutrient availability and light conditions can modify the lake water incorporated by aquatic organisms (Ladd et al., 2018; Maloney et al., 2019; Schwab et al., 2015). However, for endorheic lakes from high-altitude and semi-arid regions, lake water can be strongly modulated by evaporation, becoming isotopically ^2H-enriched, which make aquatic δ^2H from such lakes a valuable proxy for changes in relative humidity when compared to terrestrial δ^2H (Aichner et al., 2010, 2019; Mügler et al., 2008).

The recent δ^2H signal of terrestrial *n*-alkanes was evaluated in several topsoil and modern plant studies (e.g., Hepp et al., 2020; Lemma et al., 2021; Strobel et al., 2020; Struck et al., 2020), whereas the aquatic *n*-alkanes were studied along a transect of lakes in Europe (Sachse et al., 2004), and in lakes in North America (Hou

et al., 2007; Y. Huang et al., 2004) and the Tibetan Plateau (Aichner et al., 2010; Xia et al., 2008). The spatial distribution of water isotopes in lake water was also studied, for example, in Chinese lakes (Li et al., 2021). However, little is known about whether and how the δ^2H signal of terrestrial and aquatic *n*-alkanes varies spatially in lakes and how hydrological and morphological differences in a lake and the lake's catchment might modulate the δ^2H signals. This might be particularly relevant for high-altitude and semi-arid lakes, where exposition possibly produce differences in evaporation rates of the catchment and ice-cover determines the duration of aquatic biosynthesis. Moreover, the terrestrial *n*-alkanes might have time lags between their timing of formation and their deposition within the lake because of certain residence times in and transfer times through the catchment. Those transfer times can be in the order of hundreds to thousands of years and have been reported from different lacustrine systems (Aichner et al., 2021; Douglas et al., 2018; Freimuth et al., 2021; Gierga et al., 2016). However, it has been suggested to especially investigate lakes with small hydrological catchments to reduce potential time lags of terrestrial *n*-alkanes (Bliedtner et al., 2020; Gierga et al., 2016).

Here we present compound-specific δ^2H results of *n*-alkanes of 46 surface sediment samples from Lake Khar Nuur, a high-altitude and semi-arid lake in the Mongolian Altai. We explicitly choose Lake Khar Nuur because of its very small hydrological catchment to minimize transfer times of terrestrial *n*-alkanes through the catchment. We investigated the δ^2H signal of terrestrial and aquatic *n*-alkanes from the surface sediment samples to develop a better understanding about their spatial variability in the lake and potential hydrological differences. Furthermore, we analyzed the δ^2H signal of terrestrial *n*-alkanes from 13 topsoils in the Khar Nuur catchment to additionally investigate their contribution to the terrestrial *n*-alkanes in the lake and to account for hydrological differences in the lake's catchment as a result of exposition, slope and/or humidity.

2. Materials and Methods

2.1. Study Site and Sampling

Lake Khar Nuur is located in the Mongolian Altai (48°37′N, 88°56′E; Figure 1a) and was formerly described in detail by Strobel et al. (2021). Briefly, the small Lake Khar Nuur is located at high altitudes (2,486 m a.s.l), has a para-glacial origin and a small hydrological catchment (44.8 km^2) from which the lake itself covers an area of 13.8 km^2 (~31%; Figure 1b). Based on the lake's bathymetry previously published by Strobel et al. (2021), we calculated a water volume of 0.37 km^3 for the lake. Mean annual precipitation and temperature at the nearest climate station Tolbo Sum (48°25′N, 90°17′E; ~90 km SE of Lake Khar Nuur; Figures 1a and 1e) is 145 ± 35 mm and −2.4 ± 0.7°C (during the period 2009–2019; DWD Climate Data Center, 2020), respectively, and ~70% of the precipitation occurs during the summer month (June to September). Low annual temperatures lead to an ice-covered lake surface for 8–9 months per year (2016–2019; Planet Team, 2017). The modeled modern isotopic composition of precipitation (δ^2H_P) at Lake Khar Nuur reveals distinctly more negative values during winter and more positive values during summer with an annual mean of −103 ± 14‰ (Figure 1e; Table 1) (Bowen, 2021; Bowen & Revenaugh, 2003; Bowen et al., 2005).

The catchment's configuration differs for the northern and southern parts of the catchment. North-exposed flatter areas with intensively developed humus rich soils occur in the southern part of the catchment (Figures 1b and 1c). Several gullies occur in this part of the catchment, favoring, together with the underlying permafrost (Walther et al., 2017), runoff and sediment transport into the lake. The south-exposed northern parts of the catchment have steep slopes (>16°) with only very shallow developed Leptosols (Figures 1b and 1d). Residual snowfields were present in the flatter areas of the southern catchment during the summer months, producing runoff through streams by fed by snowmelt. No perennial inflow into the lake was observed in the other parts of the catchment and episodic runoff should only occur in the depth contours during snowmelt and strong precipitation events (Strobel et al., 2021). Most parts of the catchment are dominated by alpine grasses and herbs, but small patches of 50–80 cm high *Betula nana* (L.) stands cover a small area (~0.42 km^2) on a north-east exposed slope in the catchment because of favorable edaphic conditions (Figures 1b–1d) (Strobel et al., 2021).

During a fieldtrip in July 2018, we sampled the lake surface sediments (upper 0–1 cm) at 53 locations (from which we use 46 locations in this study) from the lake's floor with a Van Veen Grab sampler (Figure 1b). We took one sample from each location. In the lake's catchment, we sampled topsoils at 13 sites (Figure 1b). Although we took modern plant samples from the Khar Nuur catchment and analyzed them for their *n*-alkane distribution (Strobel et al., 2021), we did not consider them for this study because the δ^2H signal of modern plants can be

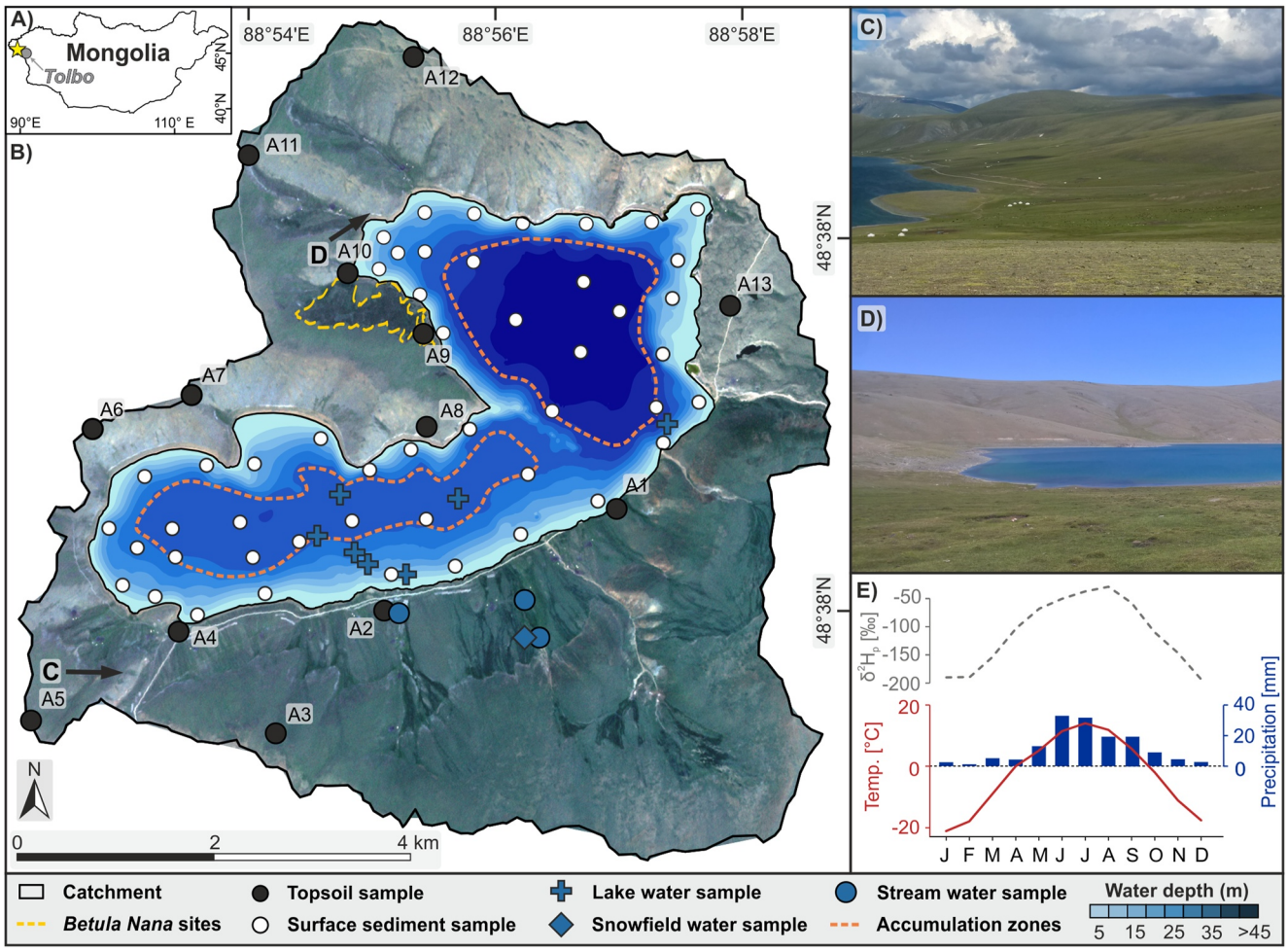

Figure 1. Overview of the study area (modified after Strobel et al. [2021]). (a) Location of the study site in western Mongolia. (b) Satellite image of the Lake Khar Nuur catchment and the lake's bathymetry. Additionally shown are the locations of the water samples (blue crosses, diamonds and dots), topsoil samples (black dots) and lake surface sediment samples (white dots). Site vegetated with Betula nana (L.) are indicated by the yellow dashed line and the accumulation zones in the lake by the orange dashed line. The viewpoint of the photos (c and d) are also shown, and the black arrows indicate their viewing direction. (c) Image of the flatter southern catchment with the intensively developed soils. (d) Image of shallow Leptosols developed on the steeper slopes in the northern part of the catchment. (e) Mean monthly temperature and precipitation composition from the nearest climate station Tolbo sum (located ~90 km SE of Khar Nuur). The modern modeled monthly hydrogen isotopic composition of precipitation (δ^2H_p) from Lake Khar Nuur is also shown in gray (data source—bathymetry [Strobel et al., 2021]; satellite image [Planet Team, 2017]; mean annual temperature and precipitation [DWD Climate Data Center, 2020]; δ^2H_p [Bowen, 2021; Bowen et al., 2005]).

affected by strong intra- and inter-annual variations (e.g., X. Huang et al., 2018; Sachse et al., 2015; Zhang et al., 2021). Topsoil samples (0–5 cm) were taken as a mixed sample of three subsamples from each site. Topsoil sample sites A1–A8 and A10–A13 mostly consist of *Poaceae* species and topsoil site A9 consists *Betula nana* (L.). Additionally, we took water samples in the southern part of the catchment from one snowfield and three streams, with two of those streams receiving source water directly from the snowfield. From the lake, we took five water samples in 2018 and two water samples in 2019 from the upper 10 cm of the water column (see Figure 1b for sample location).

2.2. Lipid Extraction and Compound-Specific δ^2H Analyzes

Lipid extraction of the topsoil and surface sediment samples (both ~10–15 g) was previously carried out and described in detail by Strobel et al. (2021). In short, total lipids were ultrasonically extracted with dichloromethane (DCM) and methanol (MeOH; 9/1, v/v). The total lipid extract was separated over aminopropyl silica gel (Supelco, 45 µm) pipette columns and further purified over coupled silvernitrate ($AgNO_3$)—zeolite (Geokleen) pipette columns. The *n*-alkanes trapped in the zeolite were subsequently dissolved in hydrofluoric acid and

Table 1
δ^2H Values of Water Samples From the Catchment and Lake Khar Nuur as Well as Modelled Mean Annual δ^2H Composition of Precipitation Derived From OPIC ([e]) (Bowen, 2021; Bowen and Revenaugh, 2003).

Material	δ^2H (‰ vs. VSMOW)
Stream[a]	−73.5
Snowfield (SF)[b]	−102.7
Stream from SF[c]	−104.8
Stream below SF[d]	−109.9
Mean lake water ($n = 7$)	−58.4 ± 4.7
Precipitation[e]	−103 ± 14

[a]See Figure 1b for location. [b]See Figure 1b for location. [c]See Figure 1b for location. [d]See Figure 1b for location. [e]Modeled mean annual δ^2H composition of precipitation at Lake Khar Nuur.

recovered by liquid-liquid extraction using hexane. Identification and quantification of the *n*-alkanes was carried out on an Agilent 7890B gas chromatograph equipped with an Agilent HP5-MS column (30 m, 320 µm, 0.25 µm film thickness) and a flame ionization detector (GC-FID), relative to external *n*-alkane standards (*n*-alkane mix C_{21}–C_{40}, Supelco).

Compound-specific δ^2H was analyzed for the terrestrial *n*-alkane C_{31} (δ^2H_{C31}) in the topsoil and surface sediment samples, whereas δ^2H of the aquatic C_{23} (δ^2H_{C23}) was analyzed in the lake surface sediments. For δ^2H of the topsoil sample A9, grown by *Betula nana* (L.), we additionally analyzed the terrestrial C_{27} since it is the dominant chain-length produced by this vegetation type in the Khar Nuur catchment (Strobel et al., 2021). The measurements were carried out on an IsoPrime visION isotope ratio mass spectrometer coupled to an Agilent 7890A GC via a GC5 pyrolysis/combustion interface operating in pyrolysis mode with a Cr (ChromeHD) reactor at 1050°C. Samples were injected splitless with a split–splitless injector. The GC was equipped with a 30 m fused silica column (HP5-MS, 0.32 mm, 0.25 µm). Each sample was measured in triplicates, except for 13 samples that were measured in duplicates (samples 03, 06, 08, 14, 21, 26, 28, 32, 34, 35, 36, 44, 45, 50, 51; see Figure 1b in Strobel et al. (2021) for sample location) due to insufficient *n*-alkane yields. δ^2H was measured against calibrated H_2 reference gas and all values are reported in per mil (‰) against VSMOW. The precision was checked by co-analyzing a standard alkane mixture (*n*-C_{27}, *n*-C_{29}, *n*-C_{33}) with known isotope composition (Arndt Schimmelmann, University of Indiana) in several concentrations, injected in duplicates every nine runs. All measurements were corrected for drift and amount dependency relative to the standard values in each sequence. Analytical precision for topsoils and lake surface sediments was <3.3‰. The analytical error for the standards was <2.0‰ ($n = 16$). The H_3^+ factor was checked every 2 days and stayed stable at 7.11 ± 0.31 during measurements. The offset between δ^2H_{C23} and δ^2H_{C31} was calculated following Equation 1 and is referred as $\Delta_{aq\text{-}terr}$ from now on.

$$\Delta_{aq\text{-}terr}[‰] = 1000 \times \left(\left[\delta^2H_{C23} + 1000\right] / \left[\delta^2H_{C31} + 1000\right] - 1 \right) \quad (1)$$

2.3. Water Sample δ^2H Analyzes

The hydrogen isotopic composition (δ^2H) of the water samples was measured in the Laboratory of Isotope Biogeochemistry Group of the Bayreuth Center of Ecology and Environmental Research (BayCEER, University of Bayreuth, Germany) using a liquid auto-sampler and thermal conversion/isotope-ratio mass-spectrometry TC-IRMS coupling (via a ConFlo IV interface, Thermo Fisher Scientific, Bremen, Germany) of a HTO pyrolysis oven (HEKAtech, Wegberg, Germany) with a Delta V Advantage IRMS (Thermo Fisher Scientific). The precision was checked by co-analyzing a standard with known isotope composition every 10 runs, which gave an analytical error of <1.2‰. Values are reported in conventional delta notation, defined as per mil (‰) against VSMOW.

2.4. Data Analyzes

The hydrological catchment of Lake Khar Nuur and its geomorphological attributes were derived from a digital elevation model (SRTM) with a spatial resolution of ~30 × 30 m. Spatial distribution maps were generated for the catchment soils (δ^2H_{C31} and δ^2H_{C27} for sites covered by alpine grasses/herbs as well as *Betula nana* (L.), respectively), δ^2H_{C31}, δ^2H_{C23}, and $\Delta_{aq\text{-}terr}$ of the lake's surface sediments using the "spline with barriers" tool in Esri ArcGIS 10.5.

3. Results

The δ^2H results of the water samples from the snowfield and two closely located streams show δ^2H values ranging from −110 to −103‰ (Table 1). A further stream, which is also located in the southern catchment, shows a more positive δ^2H value of −74‰. The lake water is even more positive with a mean δ^2H value of −58 ± 5‰ ($n = 7$; Table 1).

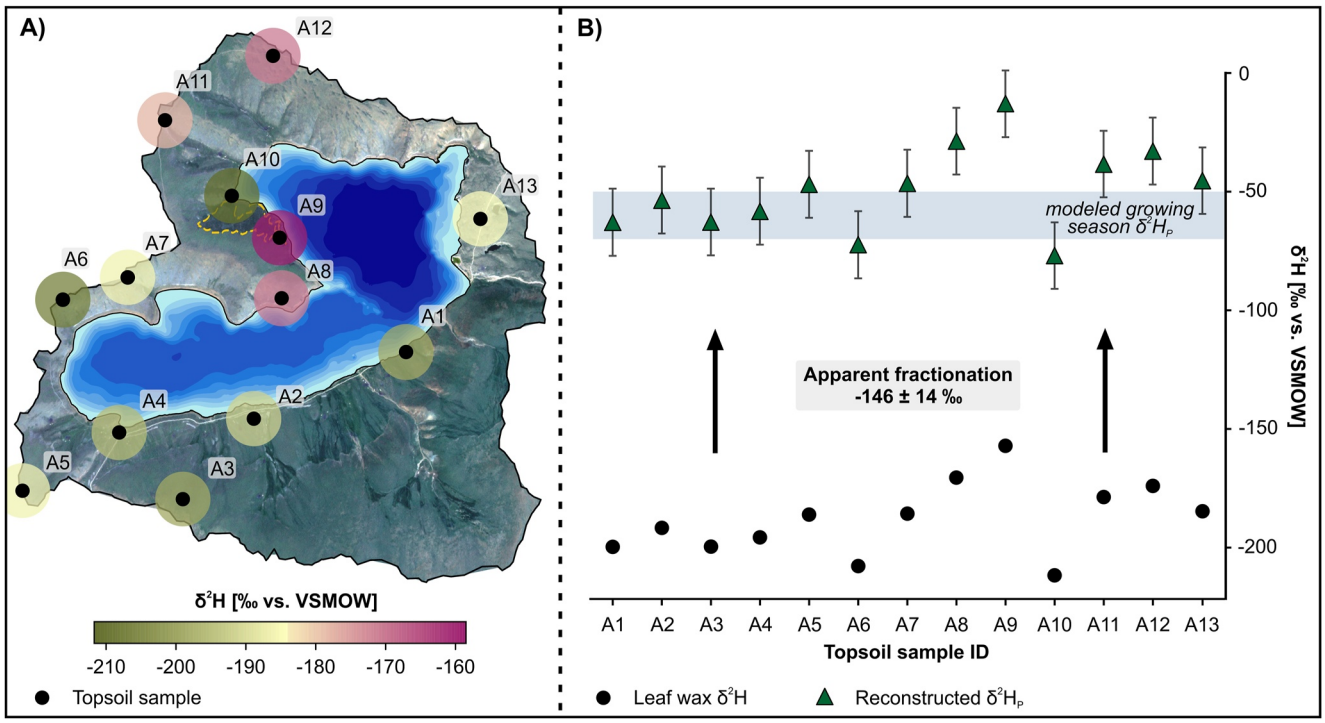

Figure 2. Compound-specific δ^2H signal of the topsoils from the Khar Nuur catchment. (a) Spatial distribution of δ^2H from the topsoils of the Khar Nuur catchment and the catchment's topography. (b) Reconstructed δ^2H_P for the catchment's topsoils by subtracting the constant apparent fractionation of 146 ± 14‰ (Struck et al., 2020) from leaf wax δ^2H from respective topsoils. The modeled growing season δ^2H_P is indicated by the blue bar and samples are classified to their location in the southern and northern part of the catchment (data source—satellite image [Planet Team, 2017]; δ^2H_P [Bowen, 2021; Bowen et al., 2005]).

The compound-specific δ^2H results of the terrestrial C_{31} of the topsoils range from −212 ± 1 to −170 ± 2‰ and generally show more negative δ^2H values for most parts of the catchment (−212 ± 1 to −185 ± 2‰), while only few samples in the northern and eastern parts of the catchment show more positive δ^2H values (−179 ± 1 to −171 ± 2‰; Figure 2a). The topsoil sample vegetated with *Betula nana* (L.) from the northern catchment with the C_{27} dominance has the most positive δ^2H value of −157 ± 1‰ (Figure 2a).

Terrestrial δ^2H_{C31} of the lake surface sediment samples shows a range of ~15‰ from −213 ± 1 to −198 ± 2‰ (Figure 3a). Although the range is small, δ^2H_{C31} values are slightly more negative along the northern shores and at two sample locations at the southern shore. Compared to δ^2H_{C31}, the aquatic δ^2H_{C23} shows generally more positive values with a distinctly larger range of ~40‰ from −188 ± 2 to −148 ± 1‰ (Figure 3b). δ^2H_{C23} values are more negative along the shorelines compared to the central parts of Lake Khar Nuur, which are more positive. The offset of δ^2H_{C23} and δ^2H_{C31} ($\Delta_{aq\text{-}terr}$) shows low values for the samples located close to the shorelines (16–56‰), whereas samples located in the central parts of the lake show distinctly higher $\Delta_{aq\text{-}terr}$ values ranging from 56 to 68‰ (Figure 3c).

4. Discussion

4.1. The δ^2H Signal in Modern Reference Material From the Khar Nuur Catchment

The majority of the topsoil samples from the Khar Nuur catchment show distinctly negative compound-specific *n*-alkane δ^2H values of −212 ± 1 to −185 ± 2‰ (Figure 2a). Terrestrial leaf waxes incorporate the δ^2H signal of the local precipitation (δ^2H_P) during the growing season through the uptake of soil water by the plants (Sachse et al., 2012). The observed *n*-alkane δ^2H values of topsoils in the Khar Nuur catchment are in good agreement with previous findings of Struck et al. (2020), who investigated δ^2H_{C31} in Mongolian topsoils. Struck et al. (2020) found that the apparent fractionation, that is, the isotopic difference of δ^2H_P and δ^2H_{C31}, is constant at −146 ± 14‰. Therefore, δ^2H_{C31} reflects δ^2H_P only slightly modulated by a constant evapo(transpi)rative enrichment (see Struck et al. [2020] for more detailed information). When subtracting this apparent fractionation factor

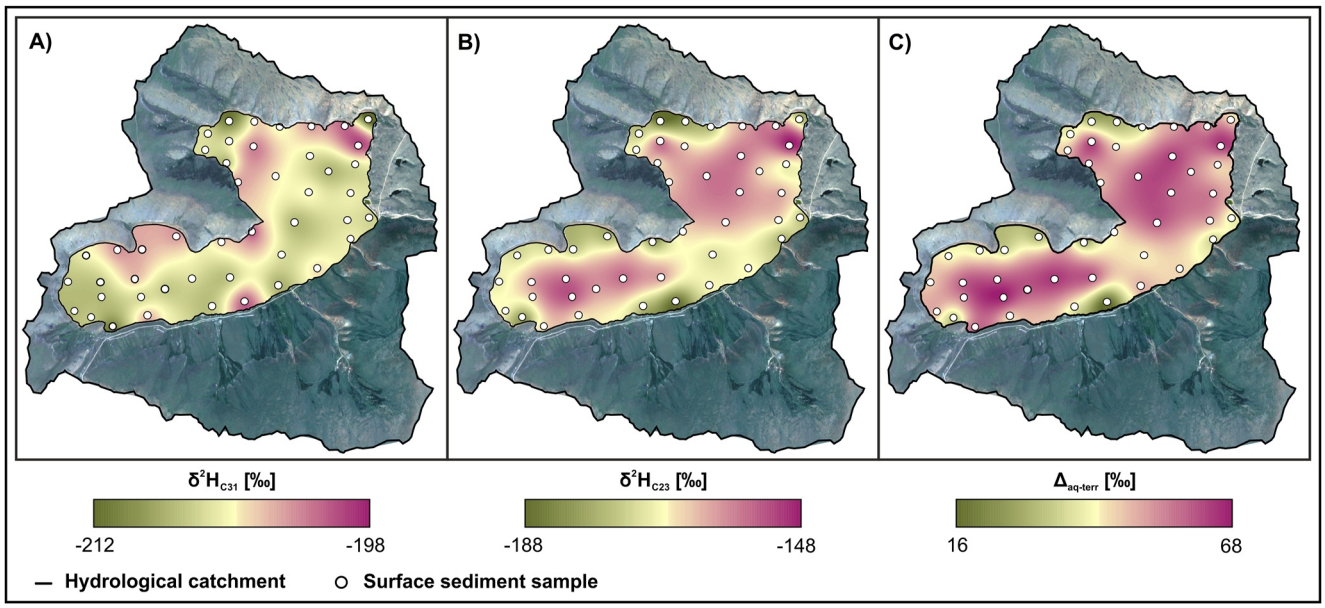

Figure 3. Compound-specific δ^2H of terrestrial and aquatic *n*-alkanes. Spatial distribution of (a) δ^2H_{C31}, (b) δ^2H_{C23}, and (c) the offset between δ^2H_{C23} and δ^2H_{C31} ($\Delta_{aq\text{-}terr}$) from the surface sediment samples of Lake Khar Nuur. The figures also show the locations of the surface sediment samples within the lake (white dots) and the catchments topography (satellite image [Planet Team, 2017]).

($-146 \pm 14‰$) from δ^2H of topsoils in the southern part of the Khar Nuur catchment, values of reconstructed δ^2H_P range from -77 ± 14 to $-45 \pm 14‰$ and agree very well with modeled local growing season precipitation, ranging from -74 to $-50‰$ (June to September; Figure 2b) (Bowen, 2021; Bowen et al., 2005). Thus, terrestrial leaf waxes in the Khar Nuur catchment most likely incorporate the δ^2H signal of the local growing season precipitation. Moreover, we have to note that residual moisture from snowmelt (i.e., a more negative winter/spring precipitation signal) can contribute to the topsoil δ^2H signal from the southern part of the catchment to a certain degree. Patches of snowfields were present in this part of the catchment during our summer sampling campaigns in 2018 and 2019. However, δ^2H values of water samples we took from a snowfield and two closely located streams (see Figure 1b for sample location) gave more negative values that are in the range of the modeled annual mean of δ^2H_P ($\sim -100‰$; see Table 1) (Bowen, 2021; Bowen & Revenaugh, 2003). Because *n*-alkane δ^2H values of the topsoils from the catchment matches with the modeled growing season δ^2H_P rather than with modeled mean annual δ^2H_P, and winter precipitation only contributes with ~30% to the annual precipitation sum (DWD Climate Data Center, 2020), we assume that *n*-alkane δ^2H is mostly dominated by growing season precipitation.

In contrast, few topsoil samples in the northern part of the catchment show more positive *n*-alkane δ^2H values (-179 ± 1 to $-157 \pm 1‰$; Samples A8, A9, A11, and A12; Figures 2a and 2b). On the one hand, southward exposition possibly favors the ^2H enrichment of soil and leaf water by elevated evapo(transpi)ration rates (Sachse et al., 2012; Zech et al., 2015). On the other hand, the shallow soils on the steep slopes have low water holding capacities for residual water and growing season precipitation at these sites. Therefore, both aspects likely explain the more positive δ^2H values of the topsoil at few sites within the catchment, which is in good agreement with previous studies similarly discussing the δ^2H signal in terrestrial leaf waxes and its modulation by soil and leaf water evapo(transpi)ration (e.g., Kahmen et al., 2013; Lemma et al., 2021; Sachse et al., 2012; Struck et al., 2020).

4.2. The δ^2H Signal in Lake Khar Nuur Surface Sediments

4.2.1. The Terrestrial δ^2H Signal

The compound-specific δ^2H signal of the terrestrial *n*-alkane C_{31} (δ^2H_{C31}) shows only small differences of ~15‰ within the Lake Khar Nuur surface sediments and is in good agreement with the majority of the *n*-alkane δ^2H values from the catchment topsoils (Figures 2 and 3a). Thus, δ^2H_{C31} in the lake surface sediments and the majority of the *n*-alkane δ^2H in the topsoils from the catchment likely reflect δ^2H_P of the growing season. Although the majority of terrestrial C_{31} *n*-alkanes with δ^2H values in the range of growing season precipitation are deposited in

the two sediment accumulation zones in the central part of the lake (Figure 1b; Strobel et al., 2021), some surface sediment samples at the shore lines are exceptional and show a divergent δ^2H signal. Samples at the northern shore show slightly more positive δ^2H_{C31} values. This could be due to the input of terrestrial *n*-alkanes from the steep slopes of the northern part of the catchment where *n*-alkane δ^2H values are possibly more positive due to exposition driven increased soil and leaf water evapo(transpi)rative enrichment. Along the southern shore, three samples show also slightly more positive δ^2H_{C31} values for this part of the lake (Figures 2a and 3a). Several gullies erode deeper and older soil material from the well-developed soils in the southern part of the catchment (Figure 2a) (Strobel et al., 2021), possibly leading to relocated terrestrial *n*-alkanes that might be aged. Those possibly relocated *n*-alkanes further might question if δ^2H_{C31} of the surface sediment samples in Lake Khar Nuur represent a contemporary signal that become deposited shortly after the *n*-alkane formation in the catchment or if those *n*-alkanes are pre-aged due to residence times in the catchment soils and/or transfer times through the catchment. Such a pre-aging of terrestrial biomarkers has been previously reported from different lakes around the world, and time lags can be in the order of hundreds to thousands years, and often strongly increase with increased anthropogenic activity in the lake catchment (Douglas et al., 2018; Freimuth et al., 2021; Gierga et al., 2016). In this context, compound-specific radiocarbon dating provide the opportunity to directly date single terrestrial *n*-alkanes. Unfortunately, surface sediment samples at Lake Khar Nuur do not provide sufficient amounts (i.e., >20 µg carbon) for precise age termination by accelerated mass spectrometry of the terrestrial chain-lengths C_{31}. Therefore, we cannot provide compound-specific age information for the terrestrial *n*-alkanes in the Khar Nuur surface sediments. However, dating modern/recent organic material is often complicated by the fact that the calibration curve flattens between ~1700 and 1950 CE and that nuclear weapon testing increased atmospheric ^{14}C dramatically after 1950 CE (Reimer et al., 2020; Schuur et al., 2016). All this can lead to quite large uncertainties in modern ^{14}C-ages. Although we cannot fully rule out the potential pre-aging of terrestrial *n*-alkanes in Lake Khar Nuur surface sediments, especially for those three shoreline samples at the southern shore, the majority of the samples should rather represent a contemporary deposition signal because of the small catchment without significant intermediate storages and the rapid transport and deposition in the accumulation zones of the Lake (Strobel et al., 2021).

4.2.2. The Aquatic δ^2H Signal

The compound-specific δ^2H signal of the aquatic *n*-alkane C_{23} (δ^2H_{C23}) reveals distinct differences in the Lake Khar Nuur surface sediments. δ^2H_{C23} is most negative at the shorelines (~−188‰) and strongly more positive (~−150‰) in the deeper basins (Figure 3b). Generally, lake water is used for synthetization of the aquatic *n*-alkanes (Aichner et al., 2019; Sachse et al., 2012), but the observed pattern of δ^2H_{C23} at Lake Khar Nuur is mostly the result of the complex climate at the study site. While the lake is ice-covered for 8–9 months, the shorelines become ice-free first and macrophytes there start to synthesize *n*-alkanes. During this early growing season, melt water and episodic runoff from winter precipitation contribute to the lake water which is used for aquatic *n*-alkane synthesis at the shorelines, and the δ^2H_{C23} signal becomes consequently more negative. Such distinctly negative δ^2H values along the shorelines due to input of isotopically negative runoff from melt water and/or precipitation were also found in modern lake water isotope analyzes in other regions (Li et al., 2021; Wu et al., 2019; Yi et al., 2008). These studies therefore support our findings at Lake Khar Nuur.

With increasing temperatures during the growing season (summer months June to September), Lake Khar Nuur becomes ice-free and macrophyte productivity strongly increases throughout the whole lake. While growing season precipitation is generally more positive compared to winter precipitation anyway, evaporation of the lake water strongly increases during the summer months. Hence, *n*-alkanes synthesized and deposited in the deeper basins and the center of the lake show a more positive δ^2H_{C23} signal that is distinctly driven by evaporative enrichment of the lake water. This is supported by lake water samples taken from Lake Khar Nuur. Compared to the stream and snowfield water samples from the catchment and modeled local mean annual δ^2H_p, the lake water is strongly more positive, that is, up to ~55‰ (Table 1). Although we only have water samples from the summer period of 2 years and the residence time of the water in the lake is not investigated, it supports our findings that the lake water used for aquatic *n*-alkane synthesis is strongly more positive due to evaporation enrichment in the endorheic Lake Khar Nuur. It is notable that *Betula* species produce also C_{23} to a certain amount in more humid regions, which might limits the interpretation of the C_{23} *n*-alkane to be solely of aquatic origin there (Hepp et al., 2019 and discussion therein). However, Strobel et al. (2021) found evidence at Lake Khar Nuur, that C_{23} is solely of aquatic origin and that the terrestrial *Betula nana* (L.) from the catchment does not contribute to the sedimentary C_{23} pool.

4.3. Paleoenvironmental Implications

Lake surface sediments from Lake Khar Nuur contain a terrestrial δ^2H_{C31} signal that mainly reflects the local growing season precipitation and an aquatic δ^2H_{C23} signal that is influenced by evaporative lake water enrichment in the deep central parts of the lake and snowmelt and runoff along the shorelines (Figures 3a and 3b). Consequently, the isotopic difference between the aquatic δ^2H_{C23} (i.e., lake water) and the terrestrial δ^2H_{C31} (i.e., growing season precipitation) can be used as valuable hydrological proxy ($\Delta_{aq\text{-}terr}$) indicating different degrees of lake water evaporation. Distinctly higher $\Delta_{aq\text{-}terr}$ values in the deeper central parts of Lake Khar Nuur indicate enhanced lake water evaporative enrichment, whereas lower $\Delta_{aq\text{-}terr}$ values of some samples at the northern shore indicate less evaporative enrichment at first sight. However, the latter samples are influenced by meltwater input and runoff as mentioned earlier (see Section 4.2.2). Lower $\Delta_{aq\text{-}terr}$ values are also shown by few samples at the central southern shore which might be due to a biased δ^2H_{C23} and δ^2H_{C31} signal by gully erosion and the input of potentially pre-aged organic material/biomarkers from this part of the catchment (see Section 4.2.1). Although differences in $\Delta_{aq\text{-}terr}$, δ^2H_{C23} and δ^2H_{C31} exist between the surface sediment samples at the shorelines and the central deeper parts of the lake, it is important to note that *n*-alkane concentrations of aquatic and terrestrial *n*-alkanes are much lower in the samples located along the shoreline compared to those of the deeper parts of the lake (Strobel et al., 2021). Therefore, the aquatic and terrestrial *n*-alkanes become preferentially deposited in the deeper basins of the lake, that is, the lake's sediment accumulation zones, and their δ^2H signal is less influenced from intra-catchment hydrological variability. While the strongly positive δ^2H_{C23} values in those accumulation zones well reflect the effect of lake water evaporative enrichment, more negative δ^2H_{C31} values mainly origin from the southern parts of the catchment and therefore well-reflect δ^2H_P of the growing season precipitation. Thus, $\Delta_{aq\text{-}terr}$ is a valuable proxy for evaporative enrichment in the semi-arid and high-altitude Lake Khar Nuur catchment and will be a great indicator for past hydrological changes when used in paleoenvironmental studies from such semi-arid lakes. Changes in the evaporative enrichment of lake water inferred by $\Delta_{aq\text{-}terr}$ were also formerly shown in surface sediment samples from semi-arid and high-altitude sites for example, from the Tibetan Plateau, where $\Delta_{aq\text{-}terr}$ values were in a similar range to Lake Khar Nuur at ~68‰ (Aichner et al., 2019; Mügler et al., 2008). Recently, Bliedtner et al. (2021) successfully applied the $\Delta_{aq\text{-}terr}$ in a first regional paleoclimate reconstruction on lake sediments from Lake Khar Nuur covering the past 4.2 ka. Lower $\Delta_{aq\text{-}terr}$ values indicate reduced evaporation rates in the Khar Nuur catchment between ~3.5 and 1.6 cal. ka BP, whereas higher $\Delta_{aq\text{-}terr}$ values indicate strongly increased evaporation after ~1.5 cal. ka BP (Bliedtner et al., 2021).

5. Conclusions

For this study, we carried out compound-specific δ^2H analyses on surface sediment samples from Lake Khar Nuur and topsoils from its catchment to investigate differences in the spatial distribution of δ^2H and potential intra-catchment hydrological variations. Our study gave the following results:

1. The majority of the topsoils in the Khar Nuur catchment have *n*-alkane δ^2H values that agree well with the modeled growing season precipitation (JJAS). Only few samples show more positive *n*-alkane δ^2H values on the steeper slopes of the northern part of the catchment. This is potentially due to southward exposition and shallower soils which potentially lead to higher evapo(transpi)ration of soil and leaf water as well as reduced water availability at these sites.
2. The δ^2H signal of the terrestrial *n*-alkane C_{31} in the surface sediments of Lake Khar Nuur shows only small variability (14‰) and is in good agreement with the δ^2H values of the topsoils. Hence, δ^2H_{31} values of the surface sediment samples most likely reflect the δ^2H signal of the growing season precipitation.
3. The aquatic *n*-alkane C_{23} shows distinctly more positive δ^2H values in the central and deepest parts of the lake, that is, the lake's sediment accumulation zones, and more negative δ^2H values along the shorelines. While the shorelines become ice-free first, the aquatic δ^2H signal there is likely influenced by isotopically negative meltwater from distinctly negative winter precipitation. The δ^2H signal in the central parts of the Lake Khar Nuur is likely the result of distinct evaporative enrichment of the lake water used for biosynthesis at those sites.
4. The isotopic offset of aquatic δ^2H_{C23} and terrestrial δ^2H_{C31} ($\Delta_{aq\text{-}terr}$) shows highest values at the center of Lake Khar Nuur because of distinct lake water evaporative enrichment. Therefore, $\Delta_{aq\text{-}terr}$ is a valuable proxy to investigate past changes in lake water evaporation, and thus past hydrological changes. While samples at the shoreline are potentially biased by intra-catchment hydrological variations, samples located in the lake's sediment accumulation zones provide consistent and robust $\Delta_{aq\text{-}terr}$ values. Therefore, our study demonstrates

that sediment retrieval for paleoenvironmental studies should carefully be constrained and be related to the sediment accumulation zones of the lake to avoid potential biases from intra-catchment hydrological variations in the catchment.

Data Availability Statement

Data used in this study are available on PANGAEA via https://doi.pangaea.de/10.1594/PANGAEA.940115.

Acknowledgments
The authors would like to thank the Ernst Abbe Stiftung for financial support of the field trip to Mongolia in 2019. P. Strobel gratefully acknowledges the support by a fellowship from the State of Thuringia (Landesgraduiertenstipendium). The authors want to thank their logistic partners in Mongolia and all field trip participants in 2018 and 2019 for their helping hands in the field. Water isotope analyses were kindly provided by Prof. G. Gebauer and his team from the Isotope Biogeochemistry Group of Bayreuth Center of Ecology and Environmental Research (BayCEER), University of Bayreuth.

References

Aichner, B., Gierga, M., Stolz, A., Mętrak, M., Wilk, M., Suska-Malawska, M., et al. (2021). Do radiocarbon ages of plant wax biomarkers agree with ^{14}C-TOC/OSL-based age models in an arid high-altitude lake system? *Radiocarbon*, *63*, 1575–1590. https://doi.org/10.1017/RDC.2021.78

Aichner, B., Herzschuh, U., Wilkes, H., Vieth, A., & Böhner, J. (2010). δD values of *n*-alkanes in Tibetan lake sediments and aquatic macrophytes – A surface sediment study and application to a 16 ka record from Lake Koucha. *Organic Geochemistry*, *41*, 779–790. https://doi.org/10.1016/j.orggeochem.2010.05.010

Aichner, B., Makhmudov, Z., Rajabov, I., Zhang, Q., Pausata, F. S. R., Werner, M., et al. (2019). Hydroclimate in the Pamirs was driven by changes in precipitation-evaporation seasonality since the last glacial period. *Geophysical Research Letters*, *46*, 13972–13983. https://doi.org/10.1029/2019gl085202

Bliedtner, M., Struck, J., Strobel, P., Salazar, G., Szidat, S., Bazarradnaa, E., et al. (2021). Late Holocene climate changes in the Altai Region based on a first high-resolution biomarker isotope record from Lake Khar Nuur. *Geophysical Research Letters*, *48*, e2021GL094299. https://doi.org/10.1029/2021gl094299

Bliedtner, M., Zech, R., Zech, J., Schäfer, I., & von Suchodoletz, H. (2020). A first Holocene leaf wax isotope-based paleoclimate record from the semi-humid to semi-arid south-eastern Caucasian lowlands. *Journal of Quaternary Science*, *35*, 625–633. https://doi.org/10.1002/jqs.3210

Bowen, G. J. (2021). *The online isotopes in precipitation calculator* (version 3.1). Retrieved from http://www.waterisotopes.org

Bowen, G. J., & Revenaugh, J. (2003). Interpolating the isotopic composition of modern meteoric precipitation. *Water Resources Research*, *39*, 1–10. https://doi.org/10.1029/2003wr002086

Bowen, G. J., Wassenaar, L. I., & Hobson, K. A. (2005). Global application of stable hydrogen and oxygen isotopes to wildlife forensics. *Oecologia*, *143*, 337–348. https://doi.org/10.1007/s00442-004-1813-y

Douglas, P. M. J., Pagani, M., Eglinton, T. I., Brenner, M., Curtis, J. H., Breckenridge, A., & Johnston, K. (2018). A long-term decrease in the persistence of soil carbon caused by ancient Maya land use. *Nature Geoscience*, *11*, 645–649. https://doi.org/10.1038/s41561-018-0192-7

DWD Climate Data Center. (2020). *Recent and historical dataset: Monthly means of precipitation totals, monthly mean air temperature and highest daily maximum temperature of a month for station Tolbo Sum (CDC-ID 44217) worldwide, version recent*. Retrieved from https://opendata.dwd.de/climate_environment/CDC/observations_global/CLIMAT/

Feakins, S. J., & Sessions, A. L. (2010). Controls on the D/H ratios of plant leaf waxes in an arid ecosystem. *Geochimica et Cosmochimica Acta*, *74*, 2128–2141. https://doi.org/10.1016/j.gca.2010.01.016

Ficken, K. J., Li, B., Swain, D. L., & Eglinton, G. (2000). An *n*-alkane proxy for the sedimentary input of submerged/floating freshwater aquatic macrophytes. *Organic Geochemistry*, *31*, 745–749. https://doi.org/10.1016/s0146-6380(00)00081-4

Freimuth, E. J., Diefendorf, A. F., Lowell, T. V., Schartman, A. K., Landis, J. D., Stewart, A. K., & Bates, B. R. (2021). Centennial-scale age offsets of plant wax *n*-alkanes in Adirondack lake sediments. *Geochimica et Cosmochimica Acta*, *300*, 119–136. https://doi.org/10.1016/j.gca.2021.02.022

Gierga, M., Hajdas, I., van Raden, U. J., Gilli, A., Wacker, L., Sturm, M., et al. (2016). Long-stored soil carbon released by prehistoric land use: Evidence from compound-specific radiocarbon analysis on Soppensee lake sediments. *Quaternary Science Reviews*, *144*, 123–131. https://doi.org/10.1016/j.quascirev.2016.05.011

Hepp, J., Schäfer, I. K., Lanny, V., Franke, J., Bliedtner, M., Rozanski, K., et al. (2020). Evaluation of bacterial glycerol dialkyl glycerol tetraether and ^{2}H–^{18}O biomarker proxies along a central European topsoil transect. *Biogeosciences*, *17*, 741–756. https://doi.org/10.5194/bg-17-741-2020

Hepp, J., Wüthrich, L., Bromm, T., Bliedtner, M., Schäfer, I. K., Glaser, B., et al. (2019). How dry was the Younger Dryas? Evidence from a coupled δ^{2}H–δ^{18}O biomarker paleohygrometer applied to the Gemündener Maar sediments, Western Eifel, Germany. *Climate of the Past*, *15*, 713–733. https://doi.org/10.5194/cp-15-713-2019

Hou, J., D'Andrea, W. J., MacDonald, D., & Huang, Y. (2007). Hydrogen isotopic variability in leaf waxes among terrestrial and aquatic plants around Blood Pond, Massachusetts (USA). *Organic Geochemistry*, *38*, 977–984. https://doi.org/10.1016/j.orggeochem.2006.12.009

Huang, X., Zhao, B., Wang, K., Hu, Y., & Meyers, P. A. (2018). Seasonal variations of leaf wax *n*-alkane molecular composition and δD values in two subtropical deciduous tree species: Results from a three-year monitoring program in central China. *Organic Geochemistry*, *118*, 15–26. https://doi.org/10.1016/j.orggeochem.2018.01.009

Huang, Y., Shuman, B., Wang, Y., & Webb, T. (2004). Hydrogen isotope ratios of individual lipids in lake sediments as novel tracers of climatic and environmental change: A surface sediment test. *Journal of Paleolimnology*, *31*, 363–375. https://doi.org/10.1023/b:jopl.0000021855.80535.13

Kahmen, A., Hoffmann, B., Schefuß, E., Arndt, S. K., Cernusak, L. A., West, J. B., & Sachse, D. (2013). Leaf water deuterium enrichment shapes leaf wax *n*-alkane δD values of angiosperm plants II: Observational evidence and global implications. *Geochimica et Cosmochimica Acta*, *111*, 50–63. https://doi.org/10.1016/j.gca.2012.09.004

Ladd, S. N., Nelson, D. B., Schubert, C. J., & Dubois, N. (2018). Lipid compound classes display diverging hydrogen isotope responses in lakes along a nutrient gradient. *Geochimica et Cosmochimica Acta*, *237*, 103–119. https://doi.org/10.1016/j.gca.2018.06.005

Lemma, B., Bittner, L., Glaser, B., Kebede, S., Nemomissa, S., Zech, W., & Zech, M. (2021). $\delta^{2}H_{n\text{-alkane}}$ and $\delta^{18}O_{sugar}$ biomarker proxies from leaves and topsoils of the Bale Mountains, Ethiopia, and implications for paleoclimate reconstructions. *Biogeochemistry*. https://doi.org/10.1007/s10533-021-00773-z

Li, Y., Tian, L., Bowen, G. J., Wu, Q., Luo, W., Chen, Y., et al. (2021). Deep lake water balance by dual water isotopes in Yungui Plateau, southwest China. *Journal of Hydrology*, *593*, 125886. https://doi.org/10.1016/j.jhydrol.2020.125886

Maloney, A. E., Nelson, D. B., Richey, J. N., Prebble, M., Sear, D. A., Hassall, J. D., et al. (2019). Reconstructing precipitation in the tropical South Pacific from dinosterol $^{2}H/^{1}H$ ratios in lake sediment. *Geochimica et Cosmochimica Acta*, *245*, 190–206. https://doi.org/10.1016/j.gca.2018.10.028

Mügler, I., Sachse, D., Werner, M., Xu, B., Wu, G., Yao, T., & Gleixner, G. (2008). Effect of lake evaporation on δD values of lacustrine *n*-alkanes: A comparison of Nam Co (Tibetan Plateau) and Holzmaar (Germany). *Organic Geochemistry*, *39*, 711–729. https://doi.org/10.1016/j.orggeochem.2008.02.008

Planet Team. (2017). *Planet application program interface: In space for life on Earth* (Vol. 2017, p. 40).

Reimer, P. J., Austin, W. E. N., Bard, E., Bayliss, A., Blackwell, P. G., Bronk Ramsey, C., et al. (2020). The IntCal20 Northern Hemisphere radiocarbon age calibration curve (0–55 cal kBP). *Radiocarbon*, *62*, 725–757. https://doi.org/10.1017/rdc.2020.41

Sachse, D., Billault, I., Bowen, G. J., Chikaraishi, Y., Dawson, T. E., Feakins, S. J., et al. (2012). Molecular paleohydrology: Interpreting the hydrogen-isotopic composition of lipid biomarkers from photosynthesizing organisms. *Annual Review of Earth and Planetary Sciences*, *40*, 221–249. https://doi.org/10.1146/annurev-earth-042711-105535

Sachse, D., Dawson, T. E., & Kahmen, A. (2015). Seasonal variation of leaf wax *n*-alkane production and $\delta^{2}H$ values from the evergreen oak tree, *Quercus agrifolia*. *Isotopes in Environmental and Health Studies*, *51*, 124–142. https://doi.org/10.1080/10256016.2015.1011636

Sachse, D., Radke, J., & Gleixner, G. (2004). Hydrogen isotope ratios of recent lacustrine sedimentary *n*-alkanes record modern climate variability. *Geochimica et Cosmochimica Acta*, *68*, 4877–4889. https://doi.org/10.1016/j.gca.2004.06.004

Schuur, E. A., Druffel, E. R., & Trumbore, S. E. (2016). *Radiocarbon and climate change: Mechanisms, applications and laboratory techniques*. Springer.

Schwab, V. F., Garcin, Y., Sachse, D., Todou, G., Séné, O., Onana, J.-M., et al. (2015). Effect of aridity on $\delta^{13}C$ and δD values of C3 plant- and C4 graminoid-derived leaf wax lipids from soils along an environmental gradient in Cameroon (Western Central Africa). *Organic Geochemistry*, *78*, 99–109. https://doi.org/10.1016/j.orggeochem.2014.09.007

Strobel, P., Haberzettl, T., Bliedtner, M., Struck, J., Glaser, B., Zech, M., & Zech, R. (2020). The potential of $\delta^{2}H_{n\text{-alkanes}}$ and $\delta^{18}O_{sugar}$ for paleoclimate reconstruction – A regional calibration study for South Africa. *Science of The Total Environment*, *716*, 137045. https://doi.org/10.1016/j.scitotenv.2020.137045

Strobel, P., Struck, J., Zech, R., & Bliedtner, M. (2021). The spatial distribution of sedimentary compounds and their environmental implications in surface sediments of Lake Khar Nuur (Mongolian Altai). *Earth Surface Processes and Landforms*, *46*, 611–625. https://doi.org/10.1002/esp.5049

Struck, J., Bliedtner, M., Strobel, P., Bittner, L., Bazarradnaa, E., Andreeva, D., et al. (2020). Leaf waxes and Hemicelluloses in topsoils reflect the $\delta^{2}H$ and $\delta^{18}O$ isotopic composition of precipitation in Mongolia. *Frontiers in Earth Science*, *8*. https://doi.org/10.3389/feart.2020.00343

Thomas, E. K., Huang, Y., Clemens, S. C., Colman, S. M., Morrill, C., Wegener, P., & Zhao, J. (2016). Changes in dominant moisture sources and the consequences for hydroclimate on the northeastern Tibetan Plateau during the past 32 kyr. *Quaternary Science Reviews*, *131*, 157–167. https://doi.org/10.1016/j.quascirev.2015.11.003

Walther, M., Dashtseren, A., Kamp, U., Temujin, K., Meixner, F., Pan, C. G., & Gansukh, Y. (2017). Glaciers, permafrost and lake levels at the Tsengel Khairkhan Massif, Mongolian Altai, during the Late Pleistocene and Holocene. *Geosciences*, *7*, 73. https://doi.org/10.3390/geosciences7030073

Wirth, S. B., & Sessions, A. L. (2016). Plant-wax D/H ratios in the southern European Alps record multiple aspects of climate variability. *Quaternary Science Reviews*, *148*, 176–191. https://doi.org/10.1016/j.quascirev.2016.07.020

Wu, H., Wu, J., Song, F., Abuduwaili, J., Saparov, A. S., Chen, X., & Shen, B. (2019). Spatial distribution and controlling factors of surface water stable isotope values ($\delta^{18}O$ and $\delta^{2}H$) across Kazakhstan, Central Asia. *Science of The Total Environment*, *678*, 53–61. https://doi.org/10.1016/j.scitotenv.2019.03.389

Xia, Z. H., Xu, B. Q., Mügler, I., Wu, G. J., Gleixner, G., Sachse, D., & Zhu, L. P. (2008). Hydrogen isotope ratios of terrigenous *n*-alkanes in lacustrine surface sediment of the Tibetan Plateau record the precipitation signal. *Geochemical Journal*, *42*, 331–338. https://doi.org/10.2343/geochemj.42.331

Yi, Y., Brock, B. E., Falcone, M. D., Wolfe, B. B., & Edwards, T. W. D. (2008). A coupled isotope tracer method to characterize input water to lakes. *Journal of Hydrology*, *350*, 1–13. https://doi.org/10.1016/j.jhydrol.2007.11.008

Zech, M., Zech, R., Rozanski, K., Gleixner, G., & Zech, W. (2015). Do *n*-alkane biomarkers in soils/sediments reflect the $\delta^{2}H$ isotopic composition of precipitation? A case study from Mt. Kilimanjaro and implications for paleoaltimetry and paleoclimate research. *Isotopes in Environmental and Health Studies*, *51*, 508–524. https://doi.org/10.1080/10256016.2015.1058790

Zhang, X., Xu, B., Günther, F., & Gleixner, G. (2021). Seasonal variation of leaf wax *n*-alkane $\delta^{2}H$ values: Differences between Quercus aquifolioides (an evergreen tree) and Stipa bungeana (a perennial grass) from the southeastern Tibetan Plateau. *Global and Planetary Change*, *207*, 103674. https://doi.org/10.1016/j.gloplacha.2021.103674